Universal Journal of Materials Science 8(2): 32-44, 2020
DOI: 10.13189/ujms.2020.080202 http://www.hrpub.org

Dirac Materials in a Matrix Way

Arka Bandyopadhyay, Debnarayan Jana*

Department of Physics, University of Calcutta, 92 Acharya Prafulla Chandra Road, Kolkata 700009, India

Received April 1, 2020; Revised May 28, 2020; Accepted June 4, 2020

Abstract Recent years have been the platform of discovery of a wide range of materials, like d-wave superconductors, graphene, and topological insulators. These materials do indeed share a fundamental similarity in their low-energy spectra namely the fermionic excitations. There carriers behave as massless Dirac particles rather than conventional fermions that obey the usual Schrödinger Hamiltonian. A surprising aspect of most Dirac materials is that many of their physical properties measured in experiments can be understood at the non-interacting level. In spite of the large effective coupling constant in case of graphene, it has been observed that the interactions do not seem to play a major key role. Controlling the electrons at Dirac nodes in the first Brillouin zone needs the interplay of sublattice symmetry, inversion symmetry and the time-reversal symmetry. In this article, we have used explicit fundamental symmetry to understand the basic features of Dirac materials occurring in three diverse systems in a compact 2×2 matrix way. Furthermore, the robustness of the Dirac cones has also been explored from the scientific notion of topological physics. In addition, an elementary introduction on the three dimensional (3D) topological insulators and d wave superconductors will shed light in their respective fields. Furthermore, we have also discussed the way to evaluate the effective mass tensor of the carriers in the two dimensional (2D) Dirac materials. This methodology has also been critically extended to three dimensional (3D) topological insulators and d wave superconductors.

Keywords Dirac Materials, Graphene, Topological Insulators, d-Wave Superconductors

1 Introduction

Two-dimensional (2D) materials [1–3] are nothing but the ultrathin nanomaterials having high degree of anisotropy as well as chemical functionality. They also possess quite diverse and exotic physical properties along with appropriate control of shape and size [4]. Dirac materials [5–7] are defined as a class of material who possess a unique Dirac-like cone type of low-energy band structure within the first Brillouin zone (BZ). This allows for the production of extraordinary electrons that are distinctive from standard electron produced in metals. Typical electrons, like those found in standard metals, tend to behave like massive particles and have a quadratic energy dependence on momentum. Such massive electrons are said to obey Schrödinger equation. Dirac electrons, on the other hand, have energies that contain a linear dependence on momentum and follow Dirac equations. Excitations in Dirac materials may be fermionic, bosonic or anyonic. The properties of these materials can be easily tailored by shifting the chemical with the help of doping or field effect setup [8–12]. In the pedagogical presentation, we would like to discuss the various symmetries associated with Dirac materials, namely graphene, topological insulators and d-wave superconductor in a simple (2×2) matrix representation.

2 Dirac cone in graphene-like materials

P.A.M Dirac [13] historically combined two major parts of physics i.e. relativity and quantum mechanics in the year 1928. It is his excellence that also predicted the new concept of spin and proposed the existence of antimatter. Furthermore, his equation has successfully introduced the brilliant idea of quantum field theory. However, the discovery of graphene [14, 15] surprisingly triggered the question regarding the relevance of relativistic Dirac equation [17–19] in the field of material science.

The nearest-neighbor tight-binding (NNTB) Hamiltonian [20, 21] of graphene can be written as

$$\hat{H} = \epsilon \sum_i c_i^\dagger c_i + t \sum_i (c_i^\dagger c_{i+1} + c_{i+1}^\dagger c_i). \qquad (1)$$

Here, i and $i+1$ label the atomic sites A and B of graphene (Fig.1) respectively. The creation (annihilation) operator $c_i^\dagger$ (c_i) creates (annihilates) an electron at i-th site. The other two terms ϵ and t represent on-site potential energy and hopping parameter of the pristine graphene respectively.

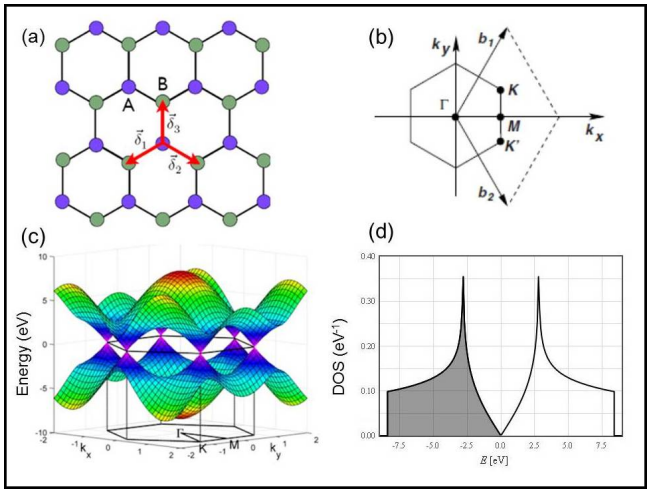

Figure 1. (a) Hexagonal structure of graphene (b) BZ of graphene (c) Semi-metallic band structure of graphene (d) V -shaped DOS near Dirac point.

In momentum space the eq.1 can be written in matrix form as

$$\hat{H} = -t \begin{pmatrix} 0 & \Delta \\ \Delta^* & 0 \end{pmatrix}. \tag{2}$$

It is to note that the uniform on-site potential energy (ϵ) i.e. the principle diagonal term of $\hat{H}$ is set to zero. This is same as shifting the Fermi energy (E_F) to zero reference value. In the above eq.2, the off-diagonal element can be written as follows

$$\Delta \equiv \sum_{\delta} \exp(i\vec{k}\cdot\vec{\delta}) \equiv \sum_{\delta} \Big(cos(\vec{k}\cdot\vec{\delta}) + i\, sin(\vec{k}\cdot\vec{\delta}) \Big). \tag{3}$$

Here, δ_i ($i \in \{1,2,3\}$) stands for the nearest-neighbor vectors. It is easy to understand from Fig.1 that

$$\delta_1 = \frac{a}{2}\Big(1, \sqrt{3}\Big), \quad \delta_2 = \frac{a}{2}\Big(1, -\sqrt{3}\Big), \quad \delta_3 = -a\Big(1, 0\Big). \tag{4}$$

The eigenvalues of the NNTB Hamiltonian in eq.2 refer the energy dispersion ($E - k$) relation of graphene sheet. The eigenvalues can be written as follows

$$E_{\pm} = \pm t\sqrt{\Delta\Delta^*} = \pm\sqrt{3 + \lambda(k)}. \tag{5}$$

A simple careful algebra in eq.5 yields

$$\lambda(k) = 2\, cos\Big(\sqrt{3}k_y a\Big) + 4\, cos\Big(\frac{3}{2}k_x a\Big)\, cos\Big(\frac{\sqrt{3}}{2}k_y a\Big). \tag{6}$$

The dispersion relations given in eq.5 have been depicted in Fig.1(c). Clearly the conduction and valence bands touch each other at corners of the BZ (K and K') giving rise to the zero band gap semiconducting or semi-metallic behaviour. This can be easily understood from the following arguments. The co-ordinates of K and K' are $\frac{2\pi}{3\sqrt{3}a}(\sqrt{3}, 1)$ and $\frac{2\pi}{3\sqrt{3}a}(\sqrt{3}, -1)$ respectively. Substituting the values of k_x and k_y individually for K and K' in eq.6 we have obtained the value of $\lambda(k)$ is invariably -3. As a consequence, $E_{\pm}$ is zero at K and K'.

Moreover, the Hamiltonian in eq.2 can be explicitly written as

$$\hat{H} = -t \sum_{\delta} \begin{pmatrix} 0 & cos(\vec{k}\cdot\vec{\delta}) + i\, sin(\vec{k}\cdot\vec{\delta}) \\ cos(\vec{k}\cdot\vec{\delta}) - i\, sin(\vec{k}\cdot\vec{\delta}) & 0 \end{pmatrix}. \tag{7}$$

Near the band touching points K and K' the eq.7 can be simplified as follows. Let us introduce two parameters $q(q_x, -q_y) = k - K$ and $q'(q_x, -q_y) = k - K'$ representing relative momentum. Therefore, the Hamiltonian can be expressed as follows

$$\begin{aligned} \hat{H}_{low} &= v_F \begin{pmatrix} 0 & q_x - iq_y \\ q_x + iq_y & 0 \end{pmatrix} \\ &= v_F \left[q_x \begin{pmatrix} 0 & 1 \\ 1 & 0 \end{pmatrix} + q_y \begin{pmatrix} 0 & -i \\ i & 0 \end{pmatrix} \right]. \end{aligned} \tag{8}$$

The above eq.8 can be written in a compact form near K and K′ point in terms of Pauli spin matrices $\sigma = (\sigma_x, \sigma_y)$)

$$\begin{aligned} K &\rightarrow \hat{H}_{low} = v_F \vec{\sigma}\cdot\vec{q} \\ K' &\rightarrow \hat{H}_{low} = v_F \vec{\sigma}\cdot\vec{q'} \end{aligned} \tag{9}$$

It is to note that these low energy Hamiltonians ($\hat{H}_{low}$) can be efficiently compared with the relativistic Dirac Hamiltonian ($\hat{H}_D$)

$$H_D = c\vec{\sigma}\cdot\vec{q} + mc^2\sigma_z = \begin{pmatrix} mc^2 & c(q_x - iq_y) \\ c(q_x + iq_y) & -mc^2 \end{pmatrix} \tag{10}$$

The eigenvalues of this massive H_D, $E_{\pm} = \pm\sqrt{q_x^2 + q_y^2 + m^2c^4}$ gives us gapped states. However, following differences can be observed.

(i) In condensed matter systems the velocity is not equal to the speed of light (c) but represents the Fermi velocity (v_F) of the system.

(ii) The mass term is zero for pristine graphene.

The quasi particles that can be described by eq.10 are popularly known as Dirac fermions. In case of massless Dirac equation $m \rightarrow 0$ the energy spectra is gapless and the dispersion relation is linear. This feature is qualitatively distinct from the quadratic dispersion of normal semiconductor

or metals. For metals and some doped semiconductors the low energy Schrödinger Hamiltonian (H_S) can be described as $H_S = p^2/2m^*$, where m^* represents effective mass of the particle. The quasiparticles that obey this description is better known as Schrödinger fermion.

Ordinary 2D materials	2D Dirac materials
Obey 2D Schrodinger equation	Obey Dirac equation in the low energy at some special point
The energy momentum dispersion relation is quadratic	The energy momentum dispersion relation is linear
$E_n = \left(n + \frac{1}{2}\right)\hbar\omega_c$ or, $E_n \propto n$	$E_n = \pm\frac{\hbar v}{l_H}\sqrt{\lvert n\rvert}$; $l_H = \sqrt{\frac{\hbar c}{eB}}$ or, $E_n \propto \sqrt{\lvert n\rvert B}$
$E_0 = \frac{1}{2}\hbar\omega_c$	$E_0 = 0$
Existence of non-zero value of the ground state energy and the value is proportional to applied magnetic field.	Existence of zero value of the ground state energy for Dirac fermion and this level is independent of cyclotron frequence and hence magnetic field.

Figure 2. Difference between normal 2D materials and 2D Dirac materials.

Furthermore, it is evident from eq.10 that the positive and negative energy eigenstates of the massive Dirac Hamiltonian are made from the same space of spinors. As a consequence, particle and hole share same effective mass (m) responsible for a band gap $\Delta = 2mc^2$. It is to remember that for normal metal and insulator particle and hole are not interconnected and satisfy Schrödinger equation separately. This leads towards different effective masses for particle and hole and there is no unique restriction on the band gap. Scanning tunneling microscope (STM) can be used to measure the density of states (DOS) experimentally. In brief, all gapless semiconductors are not Dirac materials. The differences between 2D matters and the 2D Dirac matters are described in tabular form in Fig.2. As long as they exhibit parabolic dispersion, they satisfy Schrödinger equation as depicted in Fig.3. However, Dirac materials are unique in a way that the particles are holes in these systems are always interconnected and governed by relativistic Dirac equation.

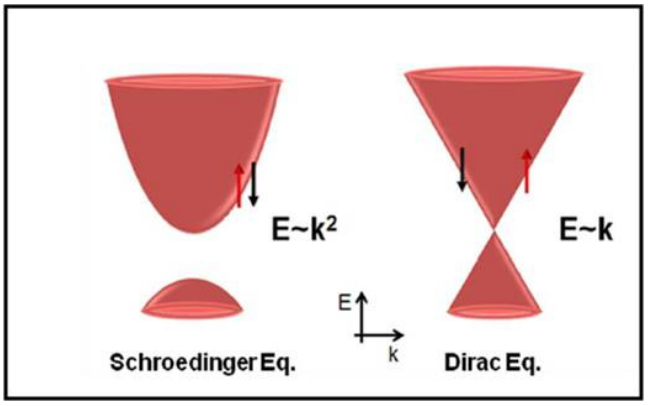

Figure 3. Energy dispersion dependence for electrons in a typical metal that tends to follow Schrödinger's Equation and have a quadratic dependence to momentum. On the right is the dispersion relation for Dirac electrons which posses a linear Dirac-like dependence.

As mentioned earlier, Dirac Hamiltonian in condensed matter systems contains the Fermi velocity instead of the speed of light. Hence, it is not Lorentz covariant. The spin operator in H_D does not correspond to the real spin of the particles but often represents some more general degree of freedom. Moreover, the bosonic Dirac materials are qualitatively different from the fermionic ones. As mentioned earlier the fermionic Dirac materials are characterized by the existence of fermionic quasiparticles where Fermi velocity is equivalent to the Dirac velocity. On the other hand, no Fermi velocity exists in bosonic Dirac materials and the Dirac velocity turns out to be a more general key property of such type of systems. Another interesting feature of Dirac materials has been described as follows. The quantization of Landau level in 2D Dirac materials is not linear in field ($\vec{B}$) but described by a relation $E_n(B) \sim \sqrt{nB}$ as depicted in Fig.4. In addition, the spacing between the quantized energy levels of the electrons in a magnetic field B changes from being linear in B for Schrödinger fermions to a $\sqrt{B}$ dependence in massless Dirac systems.

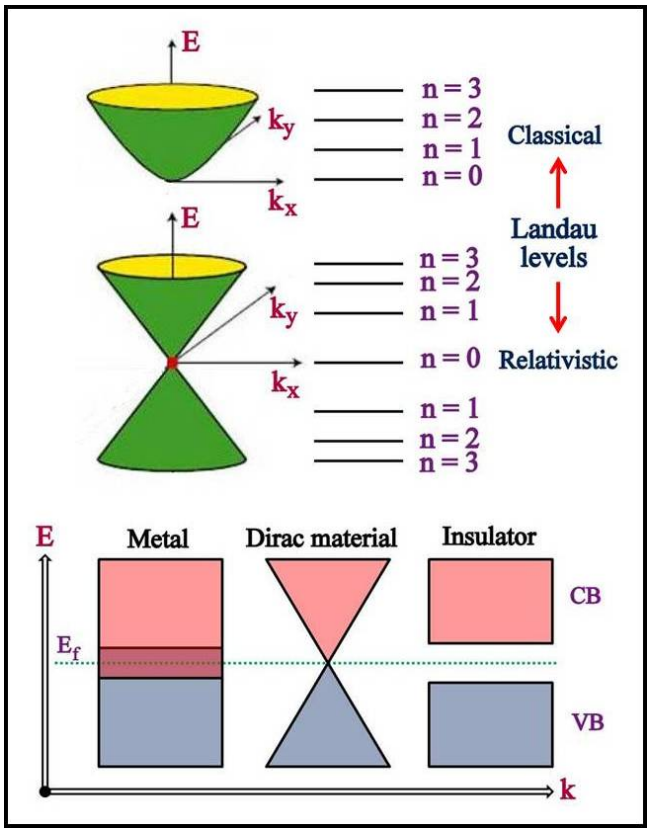

Figure 4. Comparision between the Landau levels of normal and retivistic particles (top) and Low energy excitations in usual metal, Dirac material and Insulator (bottom).

Here, it is important to note that the metals possess finite phase-space for low-energy electronic excitations where specific heat increases almost linearly with the temperature. However, semiconductors are characterized by a finite energy gap to be overcome for electronic excitations. Therefore, the thermally generated electron-hole pairs are exponentially suppressed at low temperatures. In general, the dispersion relation in arbitrary 'd' dimension can be written as $E \sim k^s$ [16]. The DOS, represented by $g(E)$ can be evaluated from elementary

calculations as given below

$$\begin{aligned} g(k)d^dk &= g(E)dE \\ or, c_d k^{d-1} g(k)dk &= g(E)dE \\ or, g(E) &= c_d \frac{d}{k^{d-1}} \frac{dk}{dE} g(k) \\ or, g(E) &= c_d \frac{d}{s} k^{d-s} g(k). \end{aligned} \tag{11}$$

This implies $g(E) \sim \frac{d}{s} E^{\frac{d}{s}-1}$. In other words, the DOS corresponding to a dispersion relation $E \sim k^s$ in 'd' dimension varies as $g(E) \sim E^{\frac{d}{s}-1}$. For Dirac materials in 'd' dimension DOS near Dirac point scales as $g(E) \sim E^{d-1}$. The DOS thus vanishes at Dirac point indicating the essential semimetal characteristic for $d > 1$. In 2D system such as graphene or topological insulators the DOS gives a V shape depicted in Fig.1(d) in comparison with the constant value for massive particles with dispersion $E = \frac{\hbar^2 k^2}{2m}$. Besides, the average energy (U) can be written as

$$U(T) = \int_0^{k_B T} E g(E) dE. \tag{12}$$

The variation of U with temperature is $U \sim T^{\frac{d}{s}+1}$. Specific heat is nothing but the energy required to change the temperature of a sample. Thus, the low temperature specific heat $\sim T^{d/s}$ in any arbitrary spatial dimension 'd'. In fact, Debye T^3 follows for $d = 3$ and $s = 1$ values. Even, ferromagnetic low temperature magnon specific $C \propto T^{3/2}$ for $d = 3$ and $s = 2$ is also indicated. The low temperature specific heat of Dirac materials $C(T \to 0) \propto T^d$ while for metal there is a uniform variation $C(T \to 0) \propto T$ Thus, for system whose relevant physical dimension greater than 1, the study of specific heat at low temperature will eventually probe the underlying nature of quasiparticles in Dirac materials. In case of graphene the parameters are $d = 2$ and $s = 1$. Therefore, $U(T) \sim T^3$ leading towards $C_v \sim T^2$.

3 Calculation of Effective Mass for Dirac-like spectrum

An important quantity in the dispersion relation $(E - k)$ is the effective mass m^* defined as

$$\frac{1}{m^*} = \frac{1}{\hbar^2} \frac{\partial^2 E}{\partial k^2} \tag{13}$$

which can be measured from the specific heat measurement. The effective mass as defined above can also be regarded as the inverse of the curvature of the band structure $E(k)$. Now, naive application of the conventional above semiconductor definition of effective mass to linear dispersion given above reduces to $(m^*)^{-1} = 0$ or an infinite effective mass of Dirac fermions [17]. Then, how is it possible to account for the finite mass (zero or non-zero, if possible) of Dirac fermions. As has been emphasized the Dirac band structure contains a linear dispersion relation $E = v_F\, p = \hbar v_F \sqrt{k_x^2 + k_y^2}$ corresponding to a constant electron speed $v = \frac{\partial E}{\partial p} = v_F$ that is. independent of the momentum. The typical Fermi velocity of graphene like material is approximately $8.3 \times 10^5\, m/s = \frac{c}{400}$, where c is the speed of light in free space. The system is not completely relativistic but the analogy is in the linear dispersion relation. Besides, in fact there is no Lorentz invariance for charge carriers in graphene. The problem of effective mass can be answered clearly if we think that the effective mass is indeed a second rank tensor $\left([(m^*)^{-1}]_{ij} = \frac{1}{\hbar^2} \nabla_i \nabla_j E(k)\right)$ and can be written more compactly for 2d graphene system [17] as

$$(m^*)^{-1} = \frac{1}{\hbar^2} \begin{pmatrix} \partial_{k_x}^2 & \partial_{k_x}\partial_{k_y} \\ \partial_{k_x}\partial_{k_y} & \partial_{k_y}^2 \end{pmatrix} \hbar v_F \sqrt{k_x^2 + k_y^2} \tag{14}$$

Substituiting the derivation in the above equation we obtain the effective mass tensor

$$(m^*)^{-1} = \frac{v_F}{\hbar} \begin{pmatrix} \frac{k_y^2}{(k_x^2+k_y^2)^{3/2}} & -\frac{k_x\, k_y}{(k_x^2+k_y^2)^{3/2}} \\ -\frac{k_x\, k_y}{(k_x^2+k_y^2)^{3/2}} & \frac{k_x^2}{(k_x^2+k_y^2)^{3/2}} \end{pmatrix}. \tag{15}$$

Further simplification of the above (2×2) matrix by the substitution $\vec{p} = \hbar\vec{k}$ along with $p = \hbar\sqrt{k_x^2 + k_y^2}$ yields

$$(m^*)^{-1} = \frac{v_F}{p^3} \begin{pmatrix} p_y^2 & -p_x\, p_y \\ -p_x\, p_y & p_x^2 \end{pmatrix} \tag{16}$$

Again 2d k-space can be further simplified by the simple trigonometric substitution $p_x = p\cos(\theta)$ and $p_y = p\sin(\theta)$ to obtain a simple form

$$\begin{aligned} (m^*)^{-1} &= \frac{v_F}{p} \begin{pmatrix} \sin^2(\theta) & -\cos(\theta)\sin(\theta) \\ -\cos(\theta)\sin(\theta) & \cos^2(\theta) \end{pmatrix} \\ &= \frac{v_F}{p}\, M(\theta) \end{aligned} \tag{17}$$

The matrix $M(\theta)$ possesses two simple but important properties which are required for finding the eigenvalues without going through secular equation. It is clear that $Tr[M(\theta)] = 1$ and $det[M(\theta)] = 0$. This gives clearly that the eigenvalues are $(0, 1)$. Hence, $(m^*)^{-1} = \frac{v_F}{p}(0, 1)$. Thus, the effective mass of Dirac electrons is $(\infty, \frac{p}{v_F}) = (m_L, m_T)$ with longitudinal mass $m_L = \infty$ while the transverse mass being $m_T = \frac{p}{v_F}$ which vanishes at the Dirac point as $p \to 0$. Considering the eigenvector of the above matrix, it can be concluded that the principal direction actually corresponds to changes in momentum parallel to the momentum direction, which is a *longitudinal* change. Note that the longitudinal mass $m_L = \infty$ is exactly the result obtained in the non-tensorial analysis. Hence, at the Dirac point electrons in graphene have an infinite longitudinal mass but are massless in transverse direction.

For n-doped graphene, there is a net excess of electrons over holes which results in states being occupied up to an energy E_F above the Dirac point. The Fermi momentum being of the linear dispersion relation turns out to be $k_F = \frac{E_F}{\hbar v_F}$. In this case, the topology of the Dirac point and Pauli exclusion principle dictate [17] that the transverse mass $m_T \approx \frac{p_F}{v_F} = \frac{E_F}{v_F^2}$, however, the longitudinal mass remains at ∞. Again, since the

effective mass is anisotropic in nature, one can compute the effective m^* as the harmonic mean [17] of all directions and is given by

$$m^*_{av} = \frac{2}{m_L^{-1} + m_T^{-1}} = \frac{2p_F}{v_F} = \frac{2E_F}{v_F^2} = 2 \times m_T \qquad (18)$$

This result also can be obtained by averaging over θ for the electrons lying within Fermi circle of radius p_F. Thus, the averaged inverse effective mass tensor is simply

$$(m^*_{av})^{-1} = \frac{v_F}{2\pi p_F} \int_0^{2\pi} M(\theta)\, d\theta \qquad (19)$$

With this definition, the averaged effective mass tensor reduces to

$$(m^*_{av})^{-1} = \frac{v_F}{p_F} \begin{pmatrix} 0, & \frac{1}{2} \end{pmatrix} \qquad (20)$$

Thus, the averaged effective mass [17] is $\frac{2E_F}{v_F^2}$ as obtained earlier. These results are important to the transport properties of these Dirac electrons in case of n-doped or p-doped graphene system. These results can be further generalized to 3d Dirac case as follows. In this case, the effective mass tensor will look like

$$(m^*)^{-1} = \frac{v_F}{p^3} \begin{pmatrix} p_y^2 + p_z^2 & -p_x\, p_y & -p_x\, p_z \\ -p_x\, p_y & p_x^2 + p_z^2 & -p_y p_z \\ -p_x\, p_z & -p_y p_z & p_x^2 + p_y^2 \end{pmatrix} \qquad (21)$$

Again 3d k-space can be further simplified by the simple trigonometric substitution $p_x = p\sin(\theta)\cos(\phi)$ and $p_y = p\sin(\theta)\sin(\phi), p_z = p\cos(\theta)$ to give us simplest form

$$(m^*)^{-1} = \frac{v_F}{p} \begin{pmatrix} \sin^2(\theta)\sin^2(\phi) + \cos^2(\theta) & -\sin^2(\theta)\cos(\phi)\sin(\phi) & -\sin(\theta)\cos(\theta)\cos(\phi) \\ -\sin^2(\theta)\cos(\phi)\sin(\phi) & \sin^2(\theta)\cos^2(\phi) + \cos^2(\theta) & -\sin(\theta)\cos(\theta)\sin(\phi) \\ -\sin(\theta)\cos(\theta)\cos(\phi) & -\sin(\theta)\cos(\theta)\sin(\phi) & \sin^2(\theta) \end{pmatrix} = \frac{v_F}{p}\, M(\theta, \phi). \qquad (22)$$

It is easy to notice again that the $Tr[M(\theta,\phi)] = 2$ and $det[M(\theta,\phi)] = 0$. It is also interesting to note that

$$M(\theta,\phi) = \begin{pmatrix} 1 & 0 & 0 \\ 0 & 0 & 0 \\ 0 & 0 & 1 \end{pmatrix} \qquad (23)$$

for $\theta = \phi = \frac{\pi}{2}$. Whereas, for $\theta = 0$ and $\phi = \frac{\pi}{2}$, $M(\theta,\phi)$ takes the form

$$M(\theta,\phi) = \begin{pmatrix} 1 & 0 & 0 \\ 0 & 1 & 0 \\ 0 & 0 & 0 \end{pmatrix} \qquad (24)$$

In the above two situations, the effective mass tensor is respectively $(\frac{p}{v_F}, \infty, \frac{p}{v_F})$ and $(\frac{p}{v_F}, \frac{p}{v_F}, \infty)$. There is only one longitudinal direction for which $m_L \to \infty$. The average effective mass $m^* = \frac{3}{(m_1)^{-1}+(m_2)^{-1}+(m_3)^{-1}} = \frac{3p_F}{v_F} = \frac{3E_F}{v_F^2}$.

In this situation, the averaged inverse effective mass tensor is simply

$$(m^*_{av})^{-1} = \frac{v_F}{4\pi p_F} \int_0^{\pi} \int_0^{2\pi} M(\theta,\phi)\ \sin(\theta) d\theta\, d\phi \qquad (25)$$

Finally, the averaged effective mass tensor reduces to

$$(m^*_{av})^{-1} = \frac{v_F}{p_F} \begin{pmatrix} \frac{2}{3} & 0 & 0 \\ 0 & \frac{2}{3} & 0 \\ 0 & 0 & \frac{2}{3} \end{pmatrix} \qquad (26)$$

with average effective mass being $\frac{3E_F}{2v_F^2}$. As a consequence, Dirac electrons behave like massless fermions which allow for ballistic transport along the surface of the Dirac material. This effective mass calculation for 3D Dirac fermions is a new result. Unlike other massless particles such as neutrinos, Dirac electrons have a charge. As a result, electrons in Dirac materials are charged massless particles that can easily be influenced by an external magnetic field. This opens the door to some exotic physics and physical properties in Dirac materials that are not found in typical materials, which may be utilized for a plethora of future applications.

The origin of the presence of Dirac nodes [18, 22] in the spectrum is due to the time-reversal symmetry and sublattice symmetry in Dirac materials. In fact. the presence of such nodes results to a sharp reduction of the phase space for low-energy excitations in these Dirac materials. In other words, the dimensionality of the set of points in momentum space where we have zero-energy excitations is reduced in Dirac materials as compared to normal metals. This shrinkage of phase space controlled by additional symmetry in the system is an indicator for Dirac materials. This phase space reduction and tailoring the symmetries involved in it can be the essential key parameter for device application. Firstly, it is possible to lift the protected symmetry of the Dirac node and therefore destroy the signature of nodes to open an energy gap. This simple modification of the spectrum of quasiparticles drastically however changes the response of the Dirac material. As a simple example, for topological insulator, the magnetic field can be important parameter for tuning the spectrum of Dirac materials. Secondly, Dirac nodes and the resultant reduction of phase space do indeed suppress dissipation and hence can be used for the devices exploiting the coherence of low-energy states in the nodes. Angle Resolved Photoemission Electron Spectroscopy (ARPES) measurements can identify the signature of Dirac nodes in the spectrum. It has been observed that the occurrence of massless Dirac fermions materials generally traces back to a material specific symmetry, which enforces degeneracy and a vanishing

mass term ($m = 0$) in the Dirac Hamiltonian.

4 Important symmetries in Dirac materials

Now let us check the associated symmetries of the Hamiltonian given in eq.8. The inversion operation can be understood as

$$\hat{I} : H(k) = \sigma_x H(-k)\sigma_x.$$

In absence of a magnetic field, the system is also naturally time-reversal invariant

$$\hat{T} : H(\vec{k}) = H^*(-\vec{k}).$$

The combination of both symmetries requires that

$$\hat{T}\hat{I} : H(\vec{k}) = \sigma_x H^*(\vec{k})\sigma_x.$$

In the above discussion we have neglected the effect of spin-orbit coupling because of its negligible value in graphene. Furthermore, it has been reported that silicene and its close relative, germanene, exhibit Dirac cones similar to graphene. All these systems are two-dimensional crystals with trigonal symmetry $\left(C_{3v}\right)$ host Dirac fermion excitations in the corners, $\vec{K}$ and $\vec{K'}$. As previously mentioned, $\hat{T}$ and $\hat{I}$ simultaneously protect the Dirac points. However, the hopping parameters can be anisotropic with different values of nearest neighbor hoppings. The presence of C_3 symmetry i.e. the symmetry after $2\pi/3$ rotation about hexagon center imposes that the hopping matrix elements must be invariant upon the cyclic changes. As a consequence, the Dirac points are restricted to the K and K′. Therefore, these three symmetries all together globally protect the Dirac points.

This trigonally symmetric structures can be efficiently used to fabricate artificial Dirac materials similar to graphene. First of all there is no sub-lattice symmetry breaking mass term in the Hamiltonian i.e $m = 0$. This is another way of saying that the pure lattice is symmetric under inversion (A $\leftrightarrow$ B). This can be understood as follows

$$\begin{aligned}\hat{I}^{-1}\hat{H}_{low}\hat{I} &= \sigma_x^{-1} v_F \begin{pmatrix} 0 & q_x - iq_y \\ q_x + iq_y & 0 \end{pmatrix} \sigma_x \\ &= v_F \begin{pmatrix} 0 & q_x - iq_y \\ q_x + iq_y & 0 \end{pmatrix} = \hat{H}_{low}.\end{aligned} \tag{27}$$

Therefore, the breaking of inversion symmetry similar to adding a σ_z term in the Dirac Hamiltonian. Next, we can check the transformation of $\hat{H}_{low}$ under time reversal operator ($\hat{T}$)

$$\begin{aligned}\hat{T}^{-1}\hat{H}_{low}\hat{T} &= \left(\sigma_y^{-1}K^{-1}\right) v_F \begin{pmatrix} 0 & q_x - iq_y \\ q_x + iq_y & 0 \end{pmatrix} \left(\sigma_y K\right) \\ &= v_F \begin{pmatrix} 0 & q_x - iq_y \\ q_x + iq_y & 0 \end{pmatrix} = \hat{H}_{low}\end{aligned} \tag{28}$$

In case of (pseudo) spin system $\hat{T} \equiv \sigma_y K$. Here, K is the complex conjugation operator. Hence, the Hamiltonian is invariant also under reversal of time. Therefore, it is easy to understand that the time-reversal symmetry along with sublattices symmetry protects the Dirac point in graphene.

5 Topological phase and associated symmetries

The first experimental observation of Integer Quantum Hall Effect (IQHE) in 1980 dramatically introduced the concept of topological phase in band theory. The topological insulating phase is completely different from conventional insulators. Here we will discuss the topologically trivial (conventional insulator) and non-trivial phase. The topological non-trivial phase is sometime referred as symmetry protected phase.

In order to distinguish topological non-trivial and trivial or normal insulating phase we have to introduce the concept of Berry phase and Chern number [23]. However, the concept of Berry phase is not specifically related to the band theory of solids but a more general concept. It deals with the quantum adiabatic transport of particles in slowly varying fields. In band theory, also, we can define a time scale corresponding to the band gap of an insulator or semiconductor. If we very slowly tune the Hamiltonian with respect to the external parameters ($\vec{R}(t)$) along a path C in parameter space. The time evolution of the state can be described by

$$H(\vec{R}(t))\,|u(t)\rangle = i\hbar\frac{d}{dt}\,|u(t)\rangle\,. \tag{29}$$

During this evolution, the systems gains a phase equivalent to

$$\theta(t) = \frac{1}{\hbar}\int_0^t E_n(\vec{R}(t'))dt' - i\int_0^t \langle n(\vec{R}(t'))|\frac{d}{dt'}|n(\vec{R}(t'))\rangle \tag{30}$$

First part can be identified as conventional dynamical phase. However, second part is known [24, 25] as negative of Berry phase γ_n. We can write

$$\begin{aligned}\gamma_n &= i\int_0^t \langle n(\vec{R}(t'))|\frac{d}{dt'}|n(\vec{R}(t'))\rangle\, dt'. \\ &= i\int_C \langle n(\vec{R})|\vec{\nabla}_{\vec{R}}|n(\vec{R})\rangle\, d\vec{R}\end{aligned} \tag{31}$$

From the analogy of the electromagnetic (EM) theory, we can write Berry connection or Berry vector potential as

$$\vec{A}_n(\vec{R}) = i\,\langle n(\vec{R})|\vec{\nabla}_{\vec{R}}|n(\vec{R})\rangle \quad \rightarrow \quad \gamma_n = \int_C \vec{A}_n(\vec{R})\cdot d\vec{R} \tag{32}$$

Applying Stokes theorem, we can write

$$\gamma_n = \int_S (\vec{\nabla}_{\vec{R}} \times \vec{A}_n(\vec{R}))\cdot d\vec{S} = \int_S \vec{F}_n \cdot d\vec{S} \tag{33}$$

$\vec{S}$ is the area in the parameter space with the boundary C. Berry curvature ($\vec{F}_n = \vec{\nabla}_{\vec{R}} \times \vec{A}_n(\vec{R})$) is simply defined as

the Berry phase per unit area in the parameter space. Berry connection (A_μ) can be thought as a n-component vector that obeys eq.32. As a consequence, Berry curvature of the i-th state ($F_{i,\mu\nu}$) turns out to be a (real) antisymmetric second-rank tensor following the relation

$$F_{i,\mu\nu}(\vec{R}) = \delta_\mu A_{i,\nu}(R) - \delta_\nu A_{i,\mu}(R) = 2Im\,\langle \delta_\mu u_i(R) | \delta_\nu u_i(R)\rangle \tag{34}$$

It can be shown that for the time reversal invariant case the Berry curvature is a odd function [23].

Furthermore, we can calculate the Chern number of the i-th state (n_i) and Hall conductance ($\sigma = \frac{e^2}{h} \times n$) as follows

$$n_i = \frac{1}{2\pi}\int_S F_{i,\mu\nu}(\vec{R}) d\vec{R} = 0. \tag{35}$$

We are integrating an odd function over a symmetric interval therefore n and hence σ have vanished. This is a signature of conventional insulators and the system is in topological trivial phase.

The low energy spectrum of graphene behaves like massless Dirac fermion. Now we are interested to find the nature of perturbations that can split the Dirac points. In our above discussion we have established that the conservation of $\hat{I}$ and $\hat{T}$ together can not open a gap. Therefore, we will now consider the Hamiltonians where either one of these symmetries is broken. Let us first add a mass term introduced by Semenov in the low energy Hamiltonian that is proportional to σ_x. Let Semenov mass term be $\delta H_{Sem} = m_{Sem}\sigma_x$. Then, the Hamiltonian in eq.8 will look like

$$\begin{aligned}\hat{H}_{Sem} &= v_F \begin{pmatrix} 0 & q_x - iq_y \\ q_x + iq_y & 0 \end{pmatrix} + m_{Sem}\begin{pmatrix} 1 & 0 \\ 0 & -1 \end{pmatrix} \\ &= \begin{pmatrix} m_{Sem} & v_F(q_x - iq_y) \\ v_F(q_x + iq_y) & -m_{Sem} \end{pmatrix}.\end{aligned} \tag{36}$$

We can now check the transformation of $\hat{H}_{Sem}$ under time reversal and inversion. At first the time reversal operation ($\hat{T}$) can be written as

$$\hat{T}^{-1}\hat{H}_{Sem}\hat{T} = \Big(\sigma_y^{-1}K^{-1}\Big)\begin{pmatrix} m_{Sem} & v_F(q_x - iq_y) \\ v_F(q_x + iq_y) & -m_{Sem} \end{pmatrix}\Big(\sigma_y K\Big) = \begin{pmatrix} m_{Sem} & v_F(q_x - iq_y) \\ v_F(q_x + iq_y) & -m_{Sem} \end{pmatrix} = \hat{H}_{Sem}. \tag{37}$$

Hence, we can see that this term is invariant under $\hat{T}$. Furthermore, the transformation of $\hat{H}_{Sem}$ under inversion operation ($\hat{I}$) can be understood as follows

$$\begin{aligned}\hat{I}^{-1}\hat{H}_{Sem}\hat{I} &= \sigma_x^{-1}\begin{pmatrix} m_{Sem} & v_F(q_x - iq_y) \\ v_F(q_x + iq_y) & -m_{Sem} \end{pmatrix}\sigma_x \\ &= -\begin{pmatrix} m_{Sem} & v_F(q_x - iq_y) \\ v_F(q_x + iq_y) & -m_{Sem} \end{pmatrix} = -\hat{H}_{Sem}.\end{aligned} \tag{38}$$

Clearly, H_{sem} changes sign under the action of $\hat{I}$. Therefore, it breaks the inversion symmetry [7] and we end up with an situation where there is nothing to protect the Dirac points. Physically, this situation is similar to choose distinct on-site potential for two different sublattices. In other words, we are choosing hexagonal boron-nitride instead of graphene. It has also been experimentally proven that the hexagonal boron-nitride has a finite band gap 6.47 eV [26]. The gap can be estimated to be $2m_{Sem}$ from the difference of eigenvalues of $\hat{H}_{Sem}$ i.e. $E_\pm = \pm\sqrt{v_F^2 q^2 + m_{Sem}^2}$. We have therefore induced a gap in the graphene spectrum. However, this case is not that interesting particularly from topological point of view. The reason is simply due to the fact that the Semenov mass δH_{sem} does not break the time reversal symmetry of the system. We have previously shown in eq. 35 that the systems remain invariant under $\hat{T}$ are topologically trivial as the Chern number remain invariably zero.

Therefore, we have to introduce an mass term that will also break the time reversal symmetry of the system and lead the system towards topologically non-trivial state. Haldane [27] historically solved the problem by introducing a mass term called Haldane mass $\delta H_{Hal} = \tau_z\sigma_z m_{Hal}$. The term δH_{Hal} is almost similar to δH_{Sem} apart form the fact that it possesses different signs in two different valleys because of the τ_z term. Therefore, the system is no longer invariant under $\hat{T}$. In order to realize the equivalent lattice model, one has to naturally introduce imaginary second nearest neighbour hopping.

We can now check the transformation of $\hat{H}_{Hal}$ under $\hat{T}$ operation

$$\hat{T}^{-1}\hat{H}_{Hal}\hat{T} = \tau_z\Big(\sigma_y^{-1}K^{-1}\Big)\begin{pmatrix} m_{Hal} & v_F(q_x - iq_y) \\ v_F(q_x + iq_y) & -m_{Hal} \end{pmatrix}\Big(\sigma_y K\Big) = -\begin{pmatrix} m_{Hal} & v_F(q_x - iq_y) \\ v_F(q_x + iq_y) & -m_{Hal} \end{pmatrix} = -\hat{H}_{Hal}. \tag{39}$$

Hence, we can see that $\hat{H}_{Hal}$ is not invariant under $\hat{T}$. Furthermore, the transformation of $\hat{H}_{Sem}$ under inversion operation ($\hat{I}$) can be understood as follows

$$\begin{aligned}\hat{I}^{-1}\hat{H}_{Hal}\hat{I} &= \tau_z\sigma_x^{-1}\begin{pmatrix} m_{Hal} & v_F(q_x - iq_y) \\ v_F(q_x + iq_y) & -m_{Hal}\end{pmatrix}\sigma_x \\ &= -\begin{pmatrix} m_{Hal} & v_F(q_x - iq_y) \\ v_F(q_x + iq_y) & -m_{Hal}\end{pmatrix} = -\hat{H}_{Hal}.\end{aligned} \tag{40}$$

Hence, the introduction of δH_{Sem} simultaneously break the $\hat{T}$ and $\hat{I}$ symmetry of the system. Similar to the previous case there is also a band gap ($= 2m_{Hal}$) in the system corresponding to the eigenvalues $E_{\pm} = \pm\sqrt{q^2 + m_{Hal}}$. Let us now calculate the Chern number of the system in presence of this Haldane mass term. For that reason, we have considered the low energy approximation of the system and argue the almost all the contribution of the eq.35 comes from the corners of the BZ. As already mentioned in eq.9 that the low energy Hamiltonian near a single Dirac point can be written as

$$H_{eff} = \vec{d}(\vec{k}) \cdot \vec{\sigma} \tag{41}$$

Therefore, $\vec{d}(\vec{k})$ can be written as $\vec{d}(\vec{k}) = (v_x k_x, v_y k_y, m)$. Thus, Berry curvature is

$$F_{x,y} = \frac{1}{2d^3}\vec{d}\cdot(\delta_i\vec{d}\times\delta_j\vec{d}) = \frac{1}{2d^3}v_x v_y m. \tag{42}$$

or,

$$n = \frac{1}{2\pi}\int_{BZ} dk_x dk_y \frac{v_x v_y m}{2(v_x^2 k_x^2 + v_y^2 k_y^2)^{3/2}} = \frac{1}{2}sgn(v_x v_y m). \tag{43}$$

At this point we want to check the values of n in presence of Semenov and Haldane mass terms.

In case of Semenov mass, valley-I corresponds to the set of input parameters $(v_x(= v_F), v_y(= v_F), m_{sem})$ while, valley-II corresponds to $(-v_x, v_y, m_{Sem})$. Substituting these set of values in eq.43 individually and then adding we get

$$n_{Sem} = \frac{1}{2}sgn(v_F^2 m_{Sem}) + \frac{1}{2}sgn(-v_F^2 m_{Sem}) = 0. \tag{44}$$

Therefore, the system is in the well expected topologically trivial state. In contrary, for the Haldane mass we can write the set of parameters for valley-I as $(v_x(= v_F), v_y(= v_F), m_{hal})$ and same for valley-II as $(-v_x, v_y, -m_{Hal})$. Hence the Chern number is

$$\begin{aligned}n_{Hal} &= \frac{1}{2}sgn(v_F^2 m_{Hal}) + \frac{1}{2}sgn(v_F^2 m_{Hal}) \\ &= sgn(m_{Hal}) = \pm 1.\end{aligned} \tag{45}$$

As v_F^2 is always positive we can remove it under sgn function. Therefore, we can conclude that graphene is a chern insulator in presence of Haldane mass. The Hall conductance is therefore $\sigma_{x,y} = \frac{e^2}{h}sgn(m_{Hal})$.

It is worth mentioning that the role of spin of electrons has not been discussed here. However, the presence of spin orbit coupling (SOC) term also allows a new spin and valley dependent mass term in the Hamiltonian. That gives rise to various important aspects of topological insulators [28]. The SOC effect is negligible for graphene while it is prominent for systems with large atomic number [29–33].

In brief, the Semenov type of mass term only transforms $\hat{H}_{low}$ to massive Dirac equation. As a result, the inversion symmetry of the system is no longer protected. However, the system remains invariant under time reversal symmetry. This effect essentially opens a gap in the energy band spectra and the system becomes insulating. This insulating phase is the conventional insulating phase of the band theory because Chern number of the phase is zero. In other words this phase is called topologically trivial phase. Whereas, the incorporation of Haldane mass term simultaneously breaks the inversion as well as time revarsal symmetry of the system. This also induces a band gap in the system while the Chern number is non zero (± 1) in this phase. Therefore, this insulating phase is distinct from the conventional insulators and we call this phase as topologically non-trivial phase. The systems with Chern numbers ± 1 are sometimes referred as Chern insulators [27, 34].

6 3D topological insulator

The formal definition of a topological insulator is an insulator in the bulk interior but the surface states are conducting. This property is a non-trivial symmetry protected by topological order. Thus the electrons in such systems move along the surface of the material. Time-reversal invariant 3D bulk insulating state can be characterized by four $\mathbb{Z}_2$ topological invariants $(\nu_0; \nu_1\nu_2\nu_3)$ [35]. We can remember that in two dimension we have only one topological invariant i.e. Chern number (n). Depending on the ν_0 value 3D TIs can be classified into two category i.e. weak and strong 3D topological insulator.

We will now briefly illustrate the underlying concept of weak and strong topological insulating phases. Let, two constraints $k_z = 0$ and $k_z = \pi$ transform the 3D Hamiltonian to 2D case with values $H(k_x, k_y, 0)$ and $H(k_x, k_y, \pi)$. We can consider, these two states as 2D topological insulators with distinct $\mathbb{Z}_2$ indices. Simply, two situations are possible

(i) The $\mathbb{Z}_2$ indices of $H(k_x, k_y, 0)$ and $H(k_x, k_y, \pi)$ are same $\rightarrow$ trivial or weak topological insulators.

and

(ii) The $\mathbb{Z}_2$ indices of $H(k_x, k_y, 0)$ and $H(k_x, k_y, \pi)$ are different $\rightarrow$ non-trivial or strong topological insulators

Therefore, the simplest way to visualize weak 3D topological insulators is to consider them as stacked 2D quantum spin Hall insulator layers as shown in Fig.5(a) and (b). This method is almost similar to the construction of 3D integer quantum

Hall states [36, 37].

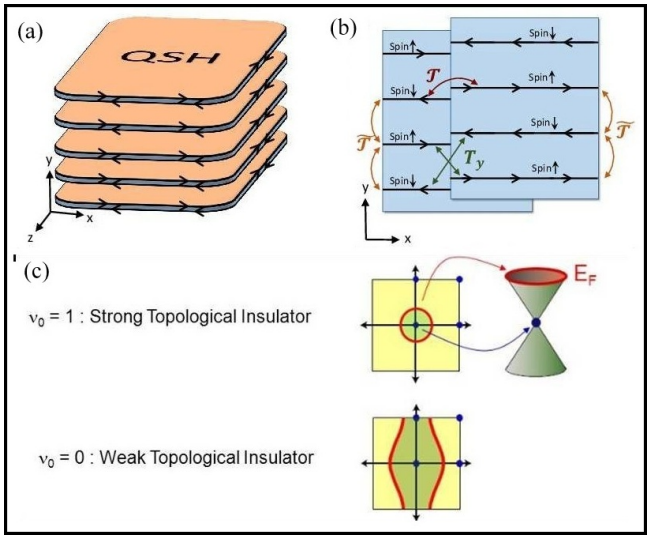

Figure 5. (a) Weak topological insulator made from quantum spin Hall layers (b) Weak topological insulator surface can be considered as bilayer. (c) Fermi circle encloses odd (even) number of Dirac points for strong (weak) topological insulator.

These layers are weakly coupled to each other and let the topological invariant of each later is described by $\nu = n$. The conductivity tensor in 3D can thus be written as follow

$$\sigma_{i,j} = \frac{e^2}{2\pi h}\epsilon_{ijk}G_k \tag{46}$$

Here, $\vec{G}$ is the the reciprocal lattice vector associated with the layers with finite uniform separation. If we increase the inter-layer coupling the surface states and Hall conductivity remain protected. Therefore, $\vec{G}$ can be indicated by three Chern numbers ($\nu_1\nu_2\nu_3$) interpreted as Miller indices in reciprocal space. The helical edge states of the coupled spin Hall insulating layers are now transformed to anisotropic surface states. However, in contrary to 2D edge states, the surface states in weak 3D TIs are not protected by time reversal symmetry. This weak topological insulating phase is characterized by $\nu_0 = 0$.

On the other hand, the $\nu_0 = 1$ phase is completely distinct from the previous case. This new phase is described as strong 3D topological insulator. The layered spin Hall insulators can not represent the strong TIs. It is to note that the surface Fermi circle in a strong topological insulator encloses an odd number of Kramer's degenerate Dirac points [23] as shown in Fig.5(c). We can immediately write down the Hamiltonian for the simplest case of one Dirac point as follows

$$\hat{H}_{sur} = i\hbar v_F \vec{\sigma}\cdot\vec{\nabla} \tag{47}$$

Here, $\hat{H}_{sur}$, $\vec{\sigma}$ and v_F represent surface Hamiltonian, spin operator and Fermi velocity respectively. The electronic states of the strong TI surface is similar to that of graphene. However there is only one significant difference. Strong TI surface exhibits one, while graphene possesses total four Dirac points considering two valleys and two spins. Therefore, the surface states of strong TIs are not spin degenerate. Time reversal symmetry imposes an elegant connection between spin and momenta. The condition that spin must rotate with momenta ($\vec{k}$) around the Fermi surface leads towards the occurrence of Berry phase with value 0 or π. In case of circling a Dirac point we achieve the Berry phase = π case.

7 d-Wave Superconductor

The superconductivity of a material occurs because of formation of electron pairs known as Cooper pairs indirectly supported by the phonon. This problem cannot be formally attacked by the perturbation theory because of the emergence of subtle non-analytic ground state of the Cooper pairs [38]. This non-perturbative condensed state was correctly described by Bardeen-Cooper-Scrieffer (BCS) theory. The wave function of a simple two particle Cooper pairs consists of orbital and spin part (α, β) as

$$\psi(\vec{r}_1, \vec{r}_2; \alpha, \beta) = \phi(\vec{r}_1, \vec{r}_2) \times \frac{1}{\sqrt{2}}\left[\alpha(1)\beta(2) - \alpha(2)\beta(1)\right] \tag{48}$$

Here the spin part being singlet in nature, the spatial part $\phi(\vec{r}_1, \vec{r}_2)$ must be symmetric to satisfy the generalized Pauli principle of antisymmetric character. One can also have other option as well i.e. orbital antisymmetric but spin part symmetric such as given by

$$\begin{aligned}\psi(\vec{r}_1, \vec{r}_2; \alpha, \beta) = \phi(\vec{r}_1, \vec{r}_2) \quad &\times \quad [\alpha(1)\alpha(2)] \\ &\times \quad [\beta(1)\beta(2)] \\ &\times \quad \frac{1}{\sqrt{2}}\left[\alpha(1)\beta(2) + \alpha(2)\beta(1)\right]\end{aligned} \tag{49}$$

Here, since three spin symmetric states are possible, hence it is named as spin triplet state. The orbital part of the wave function however can have angular momentum state such as $l = 0$ (s state), 1 (p state), 2 (d state), 3 (f state). For an effective attraction between the electrons in Cooper pair, it can be argued [39] that the singlet spin state will give the lowest ground state energy. If the spin part of the wave function is antisymmetric (Singlet), then the orbital part of the wave function has to be even ($= 0, 2, 4...$). The normal BCS Cooper pair correspond to s ($l = 0$) wave superconductor while the high temperature superconductors fall into the category of d wave superconductors with $l = 2$. The wave function in case of $l = 0$ state is spherically symmetric like the s-states of hydrogen atom. All elemental superconductors such as Al, Nb and Pb are in s-wave superconductors ($S = 0, l = 0$) while Sr_2Ru_4 is an example of p-wave ($S = 0, l = 1$) superconductor. In the same tune, cuprate high temperature superconductors are lying in d-wave ($S = 0, l = 2$) category [40]. Similarly, UPt_3, a heavy fermionic system is in the category of f-wave ($S = 1, l = 3$) superconductor.

The order parameter of this phase transition (normal to superconducting state) is a complex quantity given by the energy gap $\Delta(k) = |\Delta(k)|\exp(i\theta(k))$. Here $|\Delta(k)|$ refers to the magnitude of the superconducting gap and $\theta(k)$ is the phase of the

order parameter. Note that in the normal metallic state, this gap vanishes. This gap roughly indicates the required energy to break a Cooper pair. On the other hand the phase $\theta(k)$ is key factor which the superconducting wave function acquires spontaneously below the transition temperature T_c. Note also that this gap exists in the momentum or k-space. For an s-wave superconductor, this gap $\Delta(k)$ is independent of k and hence isotropic in all directions. Moreover, it has a fixed phase in all directions. On the otherhand, d-wave in particular $d_{x^2-y^2}$ superconductors shown in Fig.6 have anisotropic gaps and the gap can reach zero at four line nodes located at the diagonals of the BZ [41, 42].

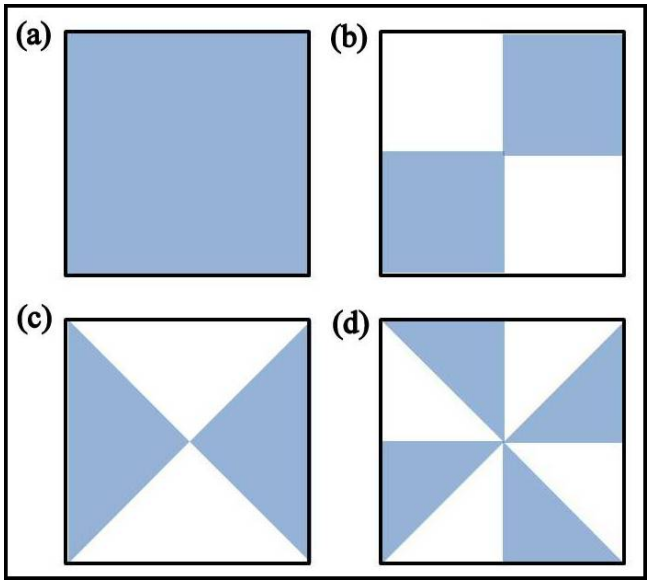

Figure 6. (a) Two dimensional superconducting state with the full symmetry of a square crystal corresponds to singlet s-wave superconductivity and the unconventional superconducting state with (b) singlet d_{xy} symmetry, (b) singlet $d_{x^2-y^2}$ symmetry and (d) singlet $g_{xy(x^2-y^2)}$ symmetry.

Thus, the energy gap of d-wave superconductors breaks the rotational symmetry in k-space. Thus, the typical d-wave pairing has cloverleaf shape with alternative positive and negative lobes. For example $d_{x^2-y^2}$ has 4 lobes with alternating phase. Since the superconducting gap of d-wave pair goes to zero in ceratin direction of k-space, hence it is easier to break up the Cooper pair with a phonon in that direction. In fact, this point really plays the key role for identifying the electronic structure with Dirac material. This fact clearly rules out the possibility of s-wave superconducters as Dirac material. In fact, one can directly visualize the sign change of the gap of d-wave superconductor by phase-referenced quasiparticle interefence technique [43]. Note that the experimental data obtained so far clearly indicate that the cuprate high temperature superconductors are two-dimensional materials. To explore the electronic structure of such a two-dimensional spin- singlet superconductor, we consider the real-space mean-field BCS Hamiltonian [18, 44, 45]

$$H_{BCS} = \sum_{\alpha} \int d^2r\ \psi^{\dagger}_{\alpha}(r)\ H_0(r)\ \psi_{\alpha}(r) + \sum_{\alpha,\beta} \int\int d^2r\ d^2r'\ \Big(\Delta_{\alpha\beta}(r,r')\ \psi^{\dagger}_{\alpha}(r)\psi^{\dagger}_{\beta}(r) + h.c.\Big) \tag{50}$$

Here $h.c.$ indicates the hermitian conjugate so that the full Hamiltonian is hermitian. The electronic field operators $\psi^{\dagger}_{\alpha}(r), \psi_{\beta}(r)$ do satisfy the following anticommutation relations given by

$$\Big\{\psi_{\alpha}(r), \psi^{\dagger}_{\beta}(r')\Big\} = \delta_{\alpha\beta}\ \delta(r-r')$$
$$\Big\{\psi^{\dagger}_{\alpha}(r), \psi^{\dagger}_{\beta}(r')\Big\} = 0 = \{\psi_{\alpha}(r), \psi_{\beta}(r')\} \tag{51}$$

The first term is usual non-interacting kinetic energy $H_0 = -\frac{\hbar^2}{2m}\nabla^2$ and the second term is responsible for the superconducting pair. It is interesting to note that the number operator $\hat{N} = \sum_{\alpha} \int d^2r\ \psi^{\dagger}_{\alpha}(r)\psi_{\alpha}(r)$ does *not* commute with the above Hamiltonian H_{BCS}. The pairing occurs below the transition temperature T_c. The spin and spatial structure of $\Delta_{\alpha\beta}$ reflects the type of superconducting pairing. For s-wave superconducting the Fourier transform of $\Delta_{\alpha\beta}$ is independent of k and hence is isotropic in nature. It does not change sign any where in the BZ. For both s-wave as well as d-wave superconductor, above T_c, $\Delta_{\alpha\beta} = 0$.

For singlet pairing, we assume $\Delta_{\alpha\beta}(r,r') = (i\sigma_y)_{\alpha\beta}\Delta(\vec{r},\vec{r}')$ and with the help of Nambu spinor $\Psi^{\dagger}(\vec{r}) = \Big(\psi^{\dagger}_{\uparrow}(r), \psi_{\downarrow}(r)\Big)$, the mean field BCS Hamiltonian can be recast [18] to

$$H_{BCS} = \iint d^2r d^2r' \begin{pmatrix} \psi^{\dagger}_{\uparrow} & \psi^{\dagger}_{\downarrow} \end{pmatrix} \begin{pmatrix} H_0 & \Delta \\ \Delta^* & -H_0 \end{pmatrix} \begin{pmatrix} \psi_{\uparrow} \\ \psi_{\downarrow} \end{pmatrix}$$
$$= \int d^2r\ \Psi^{\dagger}(r)\ \tau_z\ H_0(r)\ \Psi(r) + \iint d^2r\ d^2r'\ \Psi^{\dagger}(r)\ \tau_x\ \Delta(r,r')\ \Psi(r') \tag{52}$$

Here $\tau_i, i = x, y, z$ are Pauli matrices in Nambu space. The reduction of this Hamiltonian in this form is equivalent of Anderson's Pseudo-spin formulation [46, 47]. Finally, performing fourier transform along with converting to first quantized form, the above Hamiltonian reduces to a simple Bogolibov-deGennes (BdG) Hamiltonian [45] as

$$H_{BdG} = \epsilon_k\ \tau_z + \Delta_k\ \tau_x \tag{53}$$

where ϵ_k is the normal state band-structure energy. It is to be noted that to derive the above form, we have assumed Δ_k to be real (time-reversal symmetry) and $\epsilon_k = \epsilon_{-k}$. The diagonalization of the above Hamiltonian (53) yields

$$E_k = \sqrt{\epsilon_k^2 + |\Delta_k|^2} \tag{54}$$

The above derivation is valid for any spin-singlet superconducting order parameter including d-wave. For s-wave superconductor, however the energy gap Δ_k is real and independent of k (isotropic).

Now we would like to apply the exotic anisotropic structure of band gap of high temperature superconductor to explore the common features with Dirac materials. Now, for tetragonal cuprate superconductors because of $d_{x^2-y^2}$ wave symmetry in the CuO_2 plane, the band gap can be written [44]

$$\Delta_k = \Delta_0 \left[\cos(k_x a) - \cos(k_y a)\right] \tag{55}$$

From the above equation (55), it is evident that Δ_k vanishes along the nodal directions $|k_x| = |k_y|$ through BZ. Here Δ_k is chosen to be real to satisfy time reversal symmetry. Moreover it transforms as $x^2 - y^2$ so that it must change sign under $\pi/2$ rotation and vanish along the BZ diagonals intersecting/crossing the Fermi surface. There are four nodal points in the spectrum where the nodes cross the Fermi surface and as result $E_k = 0$. Just like the Dirac points, we can extract the low energy properties of the above quasiparticle so called *Bogolons* by expanding the equation near these nodal points. In Fig.6, we have depicted a comparison between different involved symmetries in d wave and s wave superconductors. To a first approximation, near the points of intersection between the Fermi surface and the zeros of Δ_k we assume $\epsilon_k \approx \hbar v_F\, k_\perp$ and $\Delta_k \approx \hbar\, v_\Delta\, k_\parallel$, we get the reduced massless Dirac-like Hamiltonian [18, 44] given by

$$H_D = v_F \sigma_y\, p_y + v_\Delta\, \sigma_x\, p_x. \tag{56}$$

Here, $k_\parallel$ and $k_\perp$ are respectively the deviation parallel and perpenducular to the Fermi surface. Apart from the Fermi velocity $v_F = \frac{\partial E_k}{\partial k}|_F$, we have another gap velocity $v_\Delta = \frac{\partial \Delta_k}{\partial k}|_F$ and as a result, we have obtained 2d anisotropic massless Dirac fermions rather than isotropic one in graphene. The anisotropic ratio $\frac{v_F}{v_\Delta}$ changes between different cuprate materials. Due to the presence of particle-hole symmetry of Bogoliubov spectrum, the Dirac point is situated always at the chemical potential. As a result, one needs no external fine tuning for reaching these points in d-wave superconductor. This is contrary to the situation observed in case of Dirac fermions in graphene where the chemical potential must be turned to coincide with Dirac node.

Furthermore, the effective mass (m^*) of the d-wave superconductors can be calculated as follows The eigenvalues corresponding to the Hamiltonian given in eq.56 is $E(k_x, k_y) = \hbar v_F \sqrt{k_y^2 + \alpha^2 k_x^2}$ where, α is defined as $\frac{v_\Delta}{v_F}$. Therefore, we can write

$$\begin{aligned}(m^*)^{-1} &= \frac{1}{\hbar^2}\begin{pmatrix} \partial^2_{k_x} & \partial_{k_x}\partial_{k_y} \\ \partial_{k_x}\partial_{k_x} & \partial^2_{k_x}\end{pmatrix} \hbar v_F \sqrt{k_y^2 + \alpha^2 k_x^2} \\ &= \frac{v_F \alpha^2}{(\alpha^2 p_x^2 + p_y^2)^{3/2}}\begin{pmatrix} p_y^2 & -p_x p_y \\ -p_x p_y & p_x^2\end{pmatrix}.\end{aligned} \tag{57}$$

Clearly if we substitute $\alpha = 1$ we will achieve a situation similar to graphene. Simple coordinate transformation can be performed using $p_x = p\, cos(\theta)$ and $p_y = p\, sin(\theta)$. The eq.57 can be expressed as follows

$$m^* = \frac{v_F \alpha^2 p^2}{p^3}\begin{pmatrix} \frac{sin^2(\theta)}{(\alpha^2 cos^2(\theta) + sin^2(\theta))^{3/2}} & -\frac{cos(\theta)sin(\theta)}{(\alpha^2 cos^2(\theta) + sin^2(\theta))^{3/2}} \\ -\frac{cos(\theta)sin(\theta)}{(\alpha^2 cos^2(\theta) + sin^2(\theta))^{3/2}} & \frac{cos^2(\theta)}{(\alpha^2 cos^2(\theta) + sin^2(\theta))^{3/2}}\end{pmatrix} = \frac{v_F \alpha^2}{p} M(\theta). \tag{58}$$

In the above eq.58, it can be understood that $Tr[M(\theta)] = (\alpha^2 cos^2(\theta) + sin^2(\theta))^{-3/2}$ and $det[M(\theta)] = 0$. This is also a new result for effective mass in d wave superconductors. We can recall for graphene $\alpha = 1$ and the $Tr[M(\theta)] = 1$ and $det[M(\theta)] = 0$. However, in contrary to graphene the eigenvalues of d-wave $M(\theta)$ matrix depends on θ and these are $(0,\ (\alpha^2 cos^2(\theta) + sin^2(\theta))^{-3/2})$.

Therefore, θ plays an important role in controlling the effective mass tensor. For example, $(m^*)^{-1}|_{\theta=0} = \left(0, \frac{v_F}{p\alpha}\right)$ while, $(m^*)^{-1}|_{\theta=\frac{\pi}{2}} = \left(0, \frac{v_F \alpha^2}{p}\right)$. The anisotropic effective mass can be, thus, written as $m^*|_{\theta=0} = (m_L, m_T) = \left(\infty, \frac{p\alpha}{v_F}\right)$ and $m^*|_{\theta=\frac{\pi}{2}} = (m_L, m_T) = \left(\infty, \frac{p}{v_F \alpha^2}\right)$. The average effective mass is also anisotropic with values $m^*_{av}|_{\theta=0} = \frac{2p_F\alpha}{v_F} = \frac{2E_F v_\Delta}{v_F^3}$ and $m^*_{av}|_{\theta=\frac{\pi}{2}} = \frac{2p_F}{v_F\alpha^2} = \frac{2p_F}{v_F\alpha^2} = \frac{2E_F}{v_\Delta^2}$.

Hence, we come to the conclusion that the low energy quasiparticles in d-wave superconductor are Dirac fermions (anisotropic). If the grains are arranged in a honeycomb lattice, it has been predicted [48] that the low energy spectra of 2d granular superconductors are like Bosonic Dirac system with interplay of various exotic condensed phases.

8 Conclusions

In this compacted review, we have critically discussed different symmetries viz. sublattice symmetry, inversion symmetry and the time-reversal symmetry associated with the emergence of Dirac materials. We have addressed the interconnections between three fundamental classes of Dirac materials such as graphene, topological insulator and d-wave superconductors in simple matrix representation. The linear dispersion relation of the carriers near Fermi surface is an intrinsic nature of these systems. Nevertheless, we have evaluated the effective mass tensor of the carriers near Dirac points. In the same light we have extended our calculation to the effective mass of 3D Dirac materials as well as d wave superconductors. These effective masses are highly anisotropic in nature. We have further pro-

vided a lucid introduction to the exotic field of topological band theory. We have not only distinguished different topological phases in terms of topological invariants but also discussed the role of associated symmetries in the phase transition. Because of the phase transition, the reciprocal space becomes a compact manifold leading to topological properties. Moreover, we have introduced the basic idea behind the 3D topological insulators and further classified it in strong and weak topological classes. Besides, the aspects of d wave superconductivity have been explored in the same framework of symmetry arguments. We have also evaluated the anisotropic effective mass tensor of the carriers in d wave superconductors.

Acknowledgements

Thank to Mr. Supriya Ghosal for careful reading of the manuscript.

REFERENCES

[1] N. Samarth. Condensed-matter physics: Magnetism in flatland. *Nature*, **2017**, 546, 216-218.

[2] N. Briggs, S. Subramanian, Z. Lin, X. Li, X. Zhang, K. Zhang,... L. Q. Chen. A roadmap for electronic grade 2D materials. *2D Mater.*, **2019**, 6, 022001.

[3] P. Miro, M. Audiffred, T. Heine. An Atlas of two-dimensional materials. *Chem. Soc. Rev.*, **2014**, 43, 6537-54.

[4] D. Jana, C. L. Sun, L. C. Chen, K. H. Chen. Effect of chemical doping of boron and nitrogen on the electronic, optical, and electrochemical properties of carbon nanotubes. *Prog. Mater. Sci.*, **2013**, 58, 565-635.

[5] D. Jana. 2D Materials: Future and Perspectives. *J Nanomed Res*, **2018**, 7, 00169.

[6] J. Wang, S. Deng, Z. Liu, Z. Liu, The rare two-dimensional materials with Dirac cones. *Natl. Sci. Rev.*, **2015**, 2, 22-39.

[7] S. Chowdhury, D. Jana. A theoretical review on electronic, magnetic and optical properties of silicene. *Rep. Prog. Phys.* **2016** 79, 126501.

[8] P. Nath, S. Chowdhury, D. Sanyal, D. Jana. Ab-initio calculation of electronic and optical properties of nitrogen and boron doped graphene nanosheet. *Carbon*, **2014**, 73, 275-82.

[9] S. Chowdhury, A. Bandyopadhyay, N. Dhar, D. Jana. Optical and magnetic properties of free-standing silicene, germanene and T-graphene system *Phys. Sci. Rev.*, **2017**, 2, 20165102.

[10] P. Nath, D. Sanyal, D. Jana. Ab-initio calculation of optical properties of AA-stacked bilayer graphene with tunable layer separation. *Curr. Appl. Phys.*, **2015**, 15, 691-697.

[11] C. Triola, A. Pertsova, R. S. Markiewicz, A. V Balatsky. Excitonic gap formation in pumped Dirac materials. *Phys. Rev. B*, **2017**, 95, 205410.

[12] Q. Liu, C. X. Liu, C. Xu, X. L. Qi, S. C. Zhang. Magnetic Impurities on the Surface of a Topological Insulator. *Phys. Rev. Lett.*, **2009** 102, 156603.

[13] P. A. M. Dirac. The quantum theory of the electron. *Proc. R. Soc. A*, **1928**, 117, 610.

[14] K. S. Novoselov, A. K. Geim, S. V. Morozov, D. Jiang, M. I. Katsnelson, I.V. Grigorieva... A. A. Firsov. Two-dimensional gas of massless Dirac fermions in graphene. *Nature*, **2005**, 438, 197-200.

[15] A. H. C. Neto, F. Guinea, N. M. R. Peres, K. S. Novoselov, A. K. Geim. The electronic properties of graphene. *Rev. Mod. Phys.*, 2009 81, 109.

[16] G. Montambaux. Generalized StefanBoltzmann Law. *Found. Phys.*, **2018**, 48, 395-410.

[17] C. K. Ullal, J. Shi, R. Sundararaman. Electron mobility in graphene without invoking the Dirac equation. *Am. J. Phys.*, **2019**, 87, 291.

[18] T. O. Wehling, A. M. B. Schaffer, A. V. Balatsky. Dirac materials. *Adv. Phys.*, **2014**, 76, 1-76.

[19] A. Mawrie, B. Muralidharan, Quantum thermoelectrics based on two-dimensional semi-Dirac materials. *Phys. Rev B*, **2019**, 100, 081403.

[20] A. Bandyopadhyay, A. Nandy, A. Chakrabarti, D. Jana. Optical properties and magnetic flux-induced electronic band tuning of a T-graphene sheet and nanoribbon. *Phys. Chem. Chem. Phys.* **2017**, 19, 21584-21595.

[21] S. Jana, A. Bandyopadhyay, D. Jana. Acetylenic linkage dependent electronic and optical behaviour of morphologically distinct ?ynes? *Phys. Chem. Chem. Phys.*, **2019**, 21, 13795-13808.

[22] S. Nath, A. Bandyopadhyay, S. Dutta, M. M. Uddin, D. Jana. Electronic and optical properties of non-hexagonal Dirac material S-graphene sheet and nanoribbons. *Physica E*, **2020**, 120, 114087.

[23] B. A. Bernevig, T. L. Hughes. Topological insulators and topological superconductors. **2013** (Princeton University Press) .

[24] D. J. Griffiths. Introduction to Quantum Mechanics. **2005** (Upper Saddle River, NJ: Pearson Prentice Hall).

[25] R. Shankar, Principles of Quantum Mechanics. **1995** (ISBN-0306403978. Springer).

[26] D. Wickramaratne, L. Weston, C. J. Van de Walle. Monolayer to Bulk Properties of Hexagonal Boron Nitride. *J. Phys. Chem. C*, **2018**, 122, 5524-25529.

[27] F. D. M. Haldane. Model for a Quantum Hall Effect without Landau Levels: Condensed-Matter Realization of the "Parity Anomaly". *Phys. Rev. Lett.*, **1988**, 61, 2015.

[28] C. L. Kane, E. J. Mele, Quantum Spin Hall Effect in Graphene. *Phys. Rev. Lett.*, **2005**, 95, 226801.

[29] C. C. Liu, H. Jiang, Y. G. Yao, Low-energy effective Hamiltonian involving spin-orbit coupling in silicene and two-dimensional germanium and tin. *Phys. Rev. B*, **2011**, 894, 195430.

[30] L. Chen, C. C. Liu, B. Feng, X. He, P. Cheng, Z. Ding, ... K. Wu. Evidence for Dirac Fermions in a Honeycomb Lattice Based on Silicon. *Phys. Rev. Lett*, **2012**, 109, 056804.

[31] R. G. Quhe, R. Fei, Q. Liu, J. Zheng, H. Li, C. Xu, ... J. Lu. Tunable and sizable band gap in silicene by surface adsorption. *Sci. Rep* **2012**, 2, 853.

[32] T. T. Jio, X. Y. Fan, M. M. Zheng, G. Chen. Silicene nanomeshes: bandgap opening by bond symmetry breaking and uniaxial strain. *Sci. Rep.*, **2016**, 6, 20971.

[33] A. Bandyopadhyay, D. Jana. A review on role of tetra-rings in the graphene systems and their possible applications. *Rep. Prog. Phys.*, **2020**, 83, 056501.

[34] A. Bandyopadhyay, S. Datta, D. Jana, S. Nath, M. M. Uddin. The topology and robustness of two Dirac cones in S-graphene: A tight binding approach *Sci. Rep.*, **2020**, 10, 2502.

[35] M. Z. Hasan, C. L. Kane. Colloquium: Topological insulators. *Rev. Mod. Phys.*, **2010**, 82, 3045.

[36] M. Kohmoto, B. I. Halperin, Y. S. Wu. Diophantine equation for the three-dimensional quantum Hall effect. *Phys. Rev. B*, **1992**, 45, 13488.

[37] J. L. Manes, F. Guinea, M. A. H. Vozmediano. Existence and topological stability of Fermi points in multilayered graphene. *Phys. Rev. B*, **2007**, 75, 155424.

[38] D. Jana. On Bound State of Cooper Pair in Superconductors. *Phys. Ed. (India)*, **2013**, 29, 1.

[39] M. Tinkham. Introduction to Superconductivity, **1996** (McGraw-Hill, New York) .

[40] O. Vafek, A. Vishwanath. Dirac Fermions in Solids - from High Tc cuprates and Graphene to Topological Insulators and Weyl Semimetals. *Annu. Rev. Condens. Matter Phys.*, **2014**, 5, 83.

[41] D. J. van Harlinger. Phase-sensitive tests of the symmetry of the pairing state in the high-temperature superconductors-Evidence for $d_{x^2-y^2}$ symmetry *Rev. Mod. Phys*, **1995**, 67, 515.

[42] C. C. Tsuei, J. R. Kirtley. Pairing symmetry in cuprate superconductors. *Rev. Mod. Phys.*, **2000**, 72, 969.

[43] Q. Gu, S. Wan, Q. Tang, Z. Du, H. Yang, Q. H. Wang, ... H. H. Wem. Directly visualizing the sign change of d-wave superconducting gap in $Bi_2Sr_2CaCu_2O_{8+\delta}$ by phase-referenced quasiparticle interference. *Nat. Commun.*, **2019**, 10, 1603.

[44] A. V. Balatsky, I. Vekher, J. X. Zhu. Impurity-induced states in conventional and unconventional superconductors *Rev. Mod. Phys.*, **2006**, 78, 373.

[45] P. G. De Gennes. Superconductivity of metals and alloys. **1966** (ISBN:0738201014, Cambridge, MA : Perseus).

[46] P. W. Anderson, Random-Phase Approximation in the Theory of Superconductivity. *Phys.Rev.*, **1958**, 112, 1900.

[47] D. Jana. On Anderson's Pseudo-spin Formulation of Superconductivity. *Physics Teacher*, **2006**, 48, 39.

[48] S. Banerjee, J. Fransson, A. M. B. Schaffer, H. Agren, A. V. Balatsky. Granular superconductor in a honeycomb lattice as a realization of bosonic Dirac material. *Phys. Rev. B*, **2016**, 93, 134502.

[49] J. F. Annet. Unconventional superconductivity. *Contemp. Phys.*, **1995**, 36, 423-437.